OXFORD

Human Molecular Genetics, 2017, Vol. 26, No. 15 2984–3000

doi: 10.1093/hmg/ddx189
Advance Access Publication Date: 11 May 2017
Original Article

ORIGINAL ARTICLE

Consequences of MEGF10 deficiency on myoblast function and Notch1 interactions

Madhurima Saha[1], Satomi Mitsuhashi[2,†], Michael D. Jones[1], Kelsey Manko[1], Hemakumar M. Reddy[1], Christine C. Bruels[1], Kyung-Ah Cho[1,2,‡], Christina A. Pacak[3], Isabelle Draper[4] and Peter B. Kang[1,2,5,6,*]

[1]Division of Pediatric Neurology, Department of Pediatrics, University of Florida College of Medicine, Gainesville, FL 32610, USA, [2]Department of Neurology, Boston Children's Hospital and Harvard Medical School, Boston, MA 02115, USA, [3]Child Health Research Institute, Department of Pediatrics, University of Florida College of Medicine, Gainesville, FL 32610, USA, [4]Molecular Cardiology Research Institute, Department of Medicine, Tufts Medical Center, Boston, MA 02111, USA, [5]Department of Neurology and Department of Molecular Genetics and Microbiology, University of Florida College of Medicine, Gainesville, FL 32610, USA and [6]Genetics Institute and Myology Institute, University of Florida, Gainesville, FL 32610, USA

*To whom correspondence should be addressed at: Division of Pediatric Neurology, Department of Pediatrics, University of Florida College of Medicine, PO Box 100296, Gainesville, FL 32610, USA. Tel: 352 2738920; Fax: 352 2948067; Email: pbkang@ufl.edu

Abstract

Mutations in *MEGF10* cause early onset myopathy, areflexia, respiratory distress, and dysphagia (EMARDD), a rare congenital muscle disease, but the pathogenic mechanisms remain largely unknown. We demonstrate that short hairpin RNA (shRNA)-mediated knockdown of Megf10, as well as overexpression of the pathogenic human p.C774R mutation, leads to impaired proliferation and migration of C2C12 cells. Myoblasts from *Megf10*$^{-/-}$ mice and *Megf10*$^{-/-}$*/mdx* double knockout (dko) mice also show impaired proliferation and migration compared to myoblasts from wild type and *mdx* mice, whereas the dko mice show histological abnormalities that are not observed in either single mutant mouse. Cell proliferation and migration are known to be regulated by the Notch receptor, which plays an essential role in myogenesis. Reciprocal co-immunoprecipitation studies show that Megf10 and Notch1 interact via their respective intracellular domains. These interactions are impaired by the pathogenic p.C774R mutation. Megf10 regulation of myoblast function appears to be mediated at least in part via interactions with key components of the Notch signaling pathway, and defects in these interactions may contribute to the pathogenesis of EMARDD.

Introduction

MEGF10 (Multiple EGF-like domain 10) is a type I transmembrane receptor protein that is highly expressed in developing myoblasts, muscle satellite cells, the central nervous system, and the retina (1–3). MEGF10 consists of 17 EGF-like domains in the extracellular domain (ECD), a transmembrane domain, and an intracellular domain (ICD) that includes 13 tyrosine residues. MEGF10 has two human paralogs, MEGF11 and MEGF12 (the latter is also known as PEAR1 and JEDI-1); the corresponding mouse paralogs are Megf10, Megf11, and Megf12. A single homolog to all three mammalian counterparts is found in

[†]Present address: Biomedical Informatics Laboratory, Department of Molecular Life Science, Tokai University School of Medicine, Kanagawa 259-1193, Japan.
[‡]Present address: Department of Microbiology, School of Medicine, Ewha Womans University, Seoul 07985, Republic of Korea.
Received: January 23, 2017. **Revised:** May 3, 2017. **Accepted:** May 8, 2017

Drosophila (Draper), and in *C. elegans* (CED-1) (4,5). In the central nervous system, MEGF10 contributes to the engulfment activities of glial cells (6) and participates in cell adhesion and phagocytosis (4,7). In the eye, it contributes to the formation of retinal mosaics (3).

Mutations in *MEGF10* cause an autosomal recessive skeletal muscle disorder named early onset myopathy, areflexia, respiratory distress and dysphagia (EMARDD), but notably, affected patients do not have structural or functional brain abnormalities, nor do they have visual loss or signs of neurogenic injury (8–12). Patients with compound heterozygous p.C774R and p.P442HfsX9 mutations, as well as those with two null alleles, have a severe phenotype (8), while patients with compound heterozygous p.C774R and p.C326R mutations experience a milder phenotype (9), suggesting that the p.C774R mutation is more damaging than the p.C326R mutation. The p.C774R mutation impairs tyrosine phosphorylation (13) and engulfment (14) more severely than the p.C326R mutation. In vitro (13) and in vivo (i.e., zebrafish (9) and *Drosophila* (15)) models of EMARDD have been characterized, and Megf10 is known to augment myoblast proliferation (2). Prior studies suggest that MEGF10 interacts with the highly conserved Notch signaling pathway (2,16,17), which is critical for myoblast proliferation during normal muscle development (18). Myoblasts deficient in Megf10 show decreased expression of Notch1 (2). The consequences of Megf10 impairments on a range of myoblast functions, details of the interactions between Megf10 and Notch1, and the impact of pathogenic mutations on these interactions have not been previously characterized.

The current study examines interactions between Megf10 and Notch1 in C2C12 myoblasts subjected to genetic manipulations of Megf10, and in primary myoblasts from *Megf10*$^{-/-}$ mice. The skeletal muscle phenotypes of *Megf10*$^{-/-}$ mice and *Megf10*$^{-/-}$/*mdx* double knockout (dko) mice are also examined.

Results

Megf10 deficiency impairs proliferation and migration of C2C12 myoblasts

Megf10 expression was significantly reduced in Megf10 shRNA-treated C2C12 myoblasts compared to scrambled shRNA treated cells (Supplementary Material, Fig. S1). The shRNA-treated (Megf10 and scrambled) and control myoblasts were subjected to functional assays to measure proliferation, adhesion, and migration. Megf10 deficient (shRNA treated) myoblasts showed a significant reduction in proliferation and migration compared to scrambled shRNA treated or untreated C2C12 myoblasts, with a trend towards reduced adhesion that did not reach statistical significance (Fig. 1A–D). Desmin staining (Fig. 1E) and myoblast fusion index calculations (Fig. 1F) of Megf10 shRNA treated and untreated C2C12 myoblasts revealed no significant differences, indicating that differentiation patterns are not affected by Megf10 deficiency. A TUNEL assay showed no signs of apoptosis in the Megf10 shRNA C2C12 cell line (Supplementary Material, Fig. S2).

Overexpression of the pathogenic p.C774R mutant *MEGF10* in C2C12 myoblasts results in impaired proliferation and migration

We transfected plasmids harboring wild type MEGF10 tagged with V5 as well as p.C774R and p.C326R mutant *MEGF10* into C2C12 myoblasts (Supplementary Material, Fig. S3). Transfection efficiency was confirmed by fluorescence activated cell sorting (FACS) analysis in C2C12 cells (Supplementary Material, Fig. S4). Cells expressing the p.C774R mutant displayed a significant reduction in proliferation; cells expressing the p.C326R mutant did not show significant changes (Fig. 2A and B). Myoblasts that expressed the p.C774R mutant MEGF10 showed a trend towards reduced adhesion compared to empty vector myoblasts that did not reach statistical significance (Fig. 2C). These p.C774R mutant MEGF10-overexpressing myoblasts also showed impaired migration (Fig. 2D) compared to empty vector transfected myoblasts. Cells that overexpressed the p.C326R mutant showed no significant changes, whereas overexpression of wild type Megf10 yielded enhanced proliferation and increased migration in C2C12 cells (Fig. 2A–D).

Megf10 and dystrophin double mutant mice display a severe myopathic phenotype

In the absence of exercise, *Megf10*$^{-/-}$ mice had normal mobility, and their skeletal muscles showed mildly increased endomysial connective tissue (Fig. 3A). *Mdx* mice also had a mild phenotype, with the most dramatic findings found on skeletal muscle histology (19,20). Quadriceps femoris from dko mice displayed more severe histological abnormalities compared to *mdx* mice, including pronounced fiber size variability and intracellular inclusions (Fig. 3A). Dko extensor digitorum longus (EDL), soleus, and diaphragm muscles showed similar abnormalities (Supplementary Materials, Figs S5 and S6). Trichrome staining of dko quadriceps femoris showed extensive endomysial connective tissue infiltration (Supplementary Material, Fig. S7). The dko mice developed muscle weakness, kyphosis, and a waddling gait (Fig. 3B). Hematoxylin and eosin staining demonstrated that the degree of increased centralized nuclei was similar in dko and *mdx* quadriceps femoris (Fig. 3C) and diaphragm (Supplementary Material, Fig. S6E). Immunohistochemistry demonstrated an absence of dystrophin and increased expression of utrophin (Supplementary Material, Fig. S8) in the quadriceps femoris of *mdx* and dko mice. At two months of age, the dko mice had reduced forelimb grip strength compared to *Megf10*$^{-/-}$, *mdx*, and wild type littermates (Fig. 3D). Force mechanics data showed that both EDL and soleus muscles of dko mice had reduced contractile force compared to wild type mice, but only EDL showed differences that were statistically significant for that comparison; for soleus, only *mdx* muscle had reduced contractile force compared to wild type muscle (Supplementary Material, Fig. S9).

Megf10$^{-/-}$, *mdx*, and *Megf10*$^{-/-}$/ *mdx* dko mice have decreased motor activity levels, increased muscle permeability, and fibrosis with impaired regeneration

Megf10$^{-/-}$, *mdx*, and dko mice all displayed significantly reduced motor activity compared to wild type on ActiTrack measurements after treadmill exercise, while there were no significant differences prior to exercise (Fig. 4A and B). *Mdx* and dko mice walked shorter distances on treadmill testing (Supplementary Material, Fig. S10). Dko mice showed increased fibrosis at baseline on modified Gomori trichrome stain (Supplementary Material, Fig. S7). After Evans blue dye injection, *Megf10*$^{-/-}$ mice showed mild intracellular infiltration of the dye and endomysial fibrosis, the latter on wheat germ agglutinin staining, while the dko mice exhibited more severe dye infiltration and fibrosis (Fig. 5A and B). After barium chloride injection, muscle fibers from *Megf10*$^{-/-}$ and *mdx* mice displayed a greater abundance of central nucleation and small regenerating fibers compared to wild type muscle, suggesting that muscle regeneration is occurring at a slower pace, while muscle fibers from dko mice displayed a strikingly broad distribution of fiber sizes ranging from <200

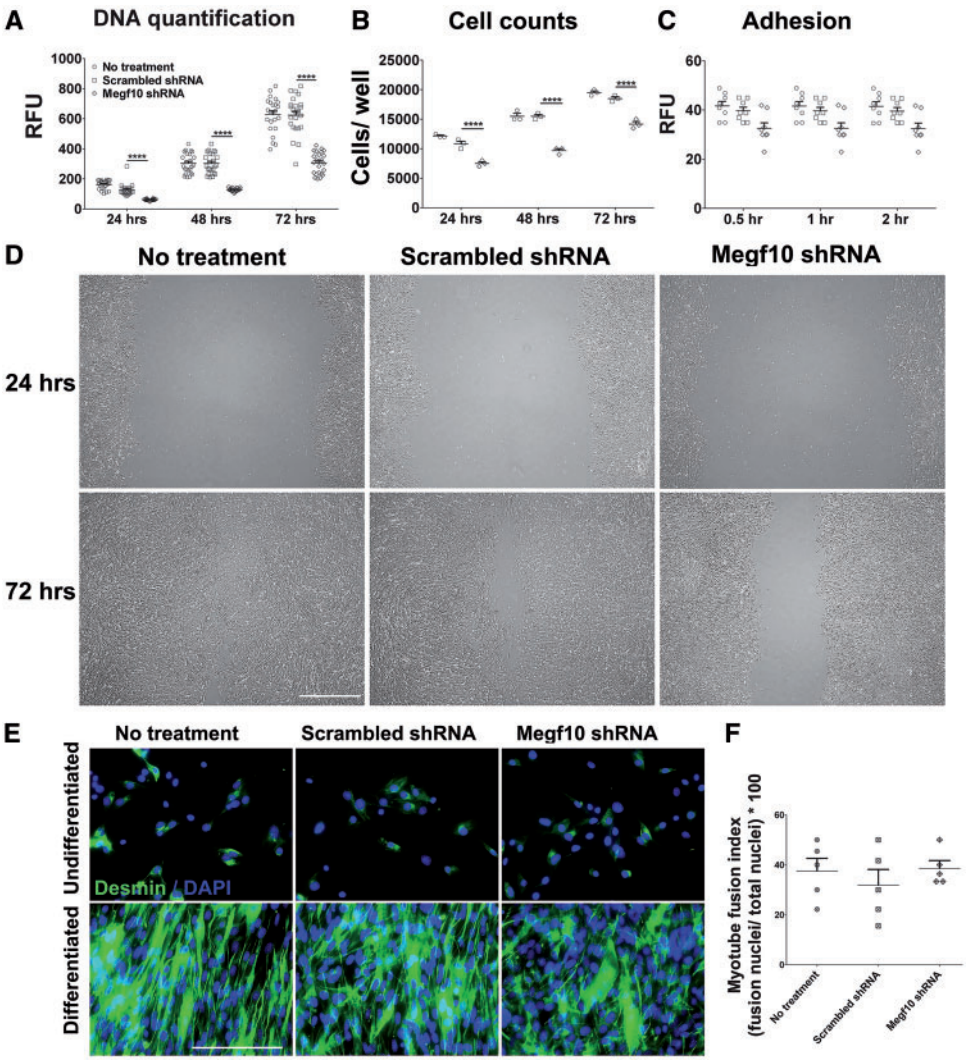

Figure 1. *Megf10* shRNA treated C2C12 cells show impairments in proliferation and migration. DNA quantification was performed using a CyQUANT kit (**A**), with scatter plots representing the mean absorbance ± S.E.M. from 24 wells in a 96-well plate; the ANOVA p value is <0.0001. Live cells were counted directly (**B**); the scatter plots represent the number of cells in each well ± S.E.M. from three independent experiments; the ANOVA p value is < 0.0001. Adhesion was assessed after the addition of calcein. The scrambled shRNA and Megf10 shRNA data for all time points were statistically significant after doing an unpaired student t test (**C**); scatter plots represent the mean fluorescence intensities of adherent cells ± S.E.M. from two independent experiments, $n = 8$; the ANOVA p value does not reach statistical significance. Photographs were taken at 24 and 72 h of culture after scratch with a 200 µl pipette tip (**D**). Ten days after switching to myogenic differentiation medium, a typical microscope field of untreated and shRNA treated C2C12 cells shows the presence of similar multinucleated myotubes for each group, defined by the presence of at least three nuclei within a cell, with positive desmin staining (**E**). The scatter plots summarize myoblast fusion index calculations from three independent experiments, each of which included the assessment of five distinct microscope fields (**F**); the ANOVA p value does not reach statistical significance. Post-test comparison results are indicated as follows: **P < 0.01; ***P < 0.001; ****P < 0.0001; RFU, relative fluorescence units; ns, not significant; scale bar, 5 mm.

µm^2 to >6,000 µm^2 with little change in central nucleation between days 5 and 12 post injury, also suggesting delayed regeneration (Fig. 5C and D).

Megf10$^{-/-}$*/mdx* dko mice display aberrant muscle fiber typing and cross-sectional areas

Fiber type analyses revealed that type I and type IIa fiber proportions in the soleus are comparable among all four strains. The EDL, in contrast, was composed almost entirely of type IIa and unstained (presumably type IIb) fibers, with the proportion of type IIa fibers higher in the *mdx* and lower in the dko mouse muscle tissues (Fig. 6A and B). Fiber size measurements showed that dko EDL and soleus muscle fibers had reduced cross-sectional areas compared to their counterparts derived from single mutant strains (Fig. 6C).

Primary myoblasts from *Megf10* deficient mice display reduced proliferation and migration

Primary myoblasts were isolated from all four mouse strains and subjected to the proliferation, adhesion, and migration assays described above. *Megf10*$^{-/-}$ and dko primary mouse myoblasts displayed a significant reduction in proliferation (Fig. 7A–C) compared to wild type and *mdx* myoblasts, correlating with the findings shown in Figures 1 and 2. Both the *Megf10*$^{-/-}$ and dko myoblasts showed a trend towards reduced adhesion compared to wild type and *mdx* myoblasts that was not statistically significant (Fig. 7D). *Megf10*$^{-/-}$ and dko primary

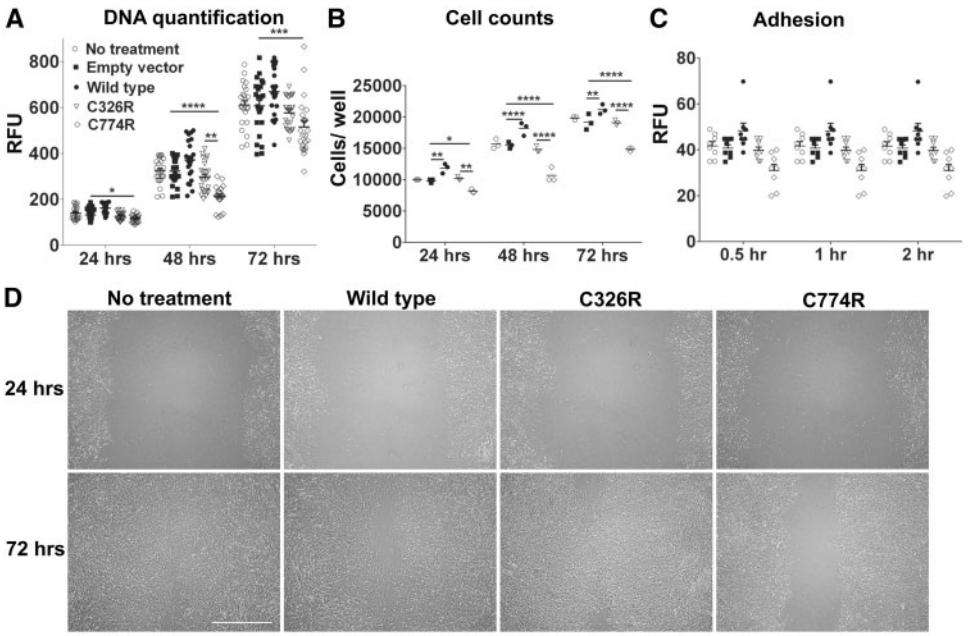

Figure 2. Overexpression of mutant p.C774R *MEGF10* suppresses C2C12 myoblast proliferation and migration compared to p.C326R mutant and control. DNA quantification was performed using a CyQUANT kit (**A**), with scatter plots representing the mean absorbance ± S.E.M. from 24 wells in a 96-well plate; the ANOVA p value is < 0.0001. Live cells were counted directly; the mean numbers of cells ± S.E.M. from three independent experiments are shown; the ANOVA p value is < 0.0001 (**B**). Adhesion was assessed after the addition of calcein; each scatter plot represents the mean fluorescence of 8 wells from a 96 well plate ± S.E.M. from two independent experiments; the ANOVA p value is 0.03 (**C**). Scratch zones were photographed at 24 and 72 h of culture after scratch with a 200 µl pipette tip (**D**). Post-test comparison results are indicated as follows: *P < 0.05; **P < 0.01; ***P < 0.001; RFU, relative fluorescence units; ns, not significant; scale bar, 5 mm.

myoblasts both displayed a significant reduction in migration compared to wild type and *mdx* myoblasts (Fig. 7E).

Notch1 interacts with Megf10

Megf10 and Notch1 protein expression rose and fell in tandem in C2C12 cells, peaking at days 3 and 4 of proliferation and dropping rapidly during differentiation (Fig. 8A). Both *Megf10*$^{-/-}$ and dko mice displayed reduced Notch1 protein expression in skeletal muscle, while *mdx* muscles showed mildly elevated levels of Megf10, and *Megf10*$^{-/-}$ muscles showed elevated levels of dystrophin (Fig. 8B and 8C). RT-PCR similarly showed reduced *Notch1* expression in *Megf10*$^{-/-}$ and dko mice, along with increased dystrophin in the *Megf10*$^{-/-}$ mice (Fig. 8D), though the reduction in Notch1 expression was not as dramatic at the RNA level as it was at the protein level (Figs 8B–D). Recombinant Megf10 was expressed in C2C12 cells, then immunoprecipitated from cell lysates. Western blot analysis of the pull down fraction using a Notch1 antibody confirmed an interaction between Megf10 and Notch1 (Fig. 8E and Supplementary Material, Fig. S11). In a reciprocal experiment, myc-tagged Notch1 was overexpressed in C2C12 cells, and cell lysates were immunoprecipitated using myc antibody, followed by western blot analysis using a Megf10 antibody (Fig. 8F).

Simultaneous knockdown of Megf10 and Notch1 does not impair cell proliferation more severely than knockdown of Megf10 alone

Simultaneous knockdown of Megf10 via shRNA and Notch1 via siRNA was confirmed via western blot (Fig. 8G). Based on DNA quantification and cell counts, the single knockdown and double knockdown myoblasts all showed defects in proliferation compared to no treatment and scrambled shRNA myoblasts (Fig. 8H). Notch1 localizes to the sarcolemma in the quadriceps femoris muscle of wild type mice, and this staining was reduced in the same muscles from *Megf10*$^{-/-}$ and dko mice (Fig. 8I). These findings are consistent with protein (Fig. 8C) and RNA (Fig. 8D) expression data levels observed in the same muscle type of these mouse strains. Immunohistochemical analysis of quadriceps femoris muscle sections from all four mouse strains using Notch1 and Megf10 antibodies showed colocalization both visually (Supplementary Material, Fig. S12A) and quantitatively (Supplementary Material, Fig. S12B).

The ICD of Megf10 interacts with Notch1

To determine which domain of Megf10 interacts with Notch1, the delta/serrate/LAG-2 (DSL) domain, ECD, and ICD were cloned, ligated into a glutathione S-transferase (GST)-tagged construct, and transfected into wild type C2C12 cells (Fig. 9A). After performing a glutathione-S-transferase (GST) interaction assay with the GST-tagged delta/serrate/LAG-2 (DSL) domain, ECD, and ICD of Megf10, Notch1 was found to interact only with the ICD of Megf10 (Fig. 9B). In reciprocal experiments, immunoprecipitation of myc-tagged Notch1 was followed by immunoblotting for GST (Fig. 9C). These findings were further corroborated by immunoprecipitation of a flag-tagged ICD of Notch1 (NICD1), which was found to interact with the V5-tagged MEGF10 (Fig. 9D). Immunofluorescence studies of Megf10 and Notch1 in wild type and C2C12 cells using antibodies targeted to the ICDs of both proteins suggest that Megf10 localizes to the cell membrane, while Notch1 localizes to both the cell membrane and the nucleus (Fig. 9E and Supplementary Material, Fig. S13A). Quantification of the fluorescence signals supports the co-localization of Megf10 and Notch 1 (Supplementary Material,

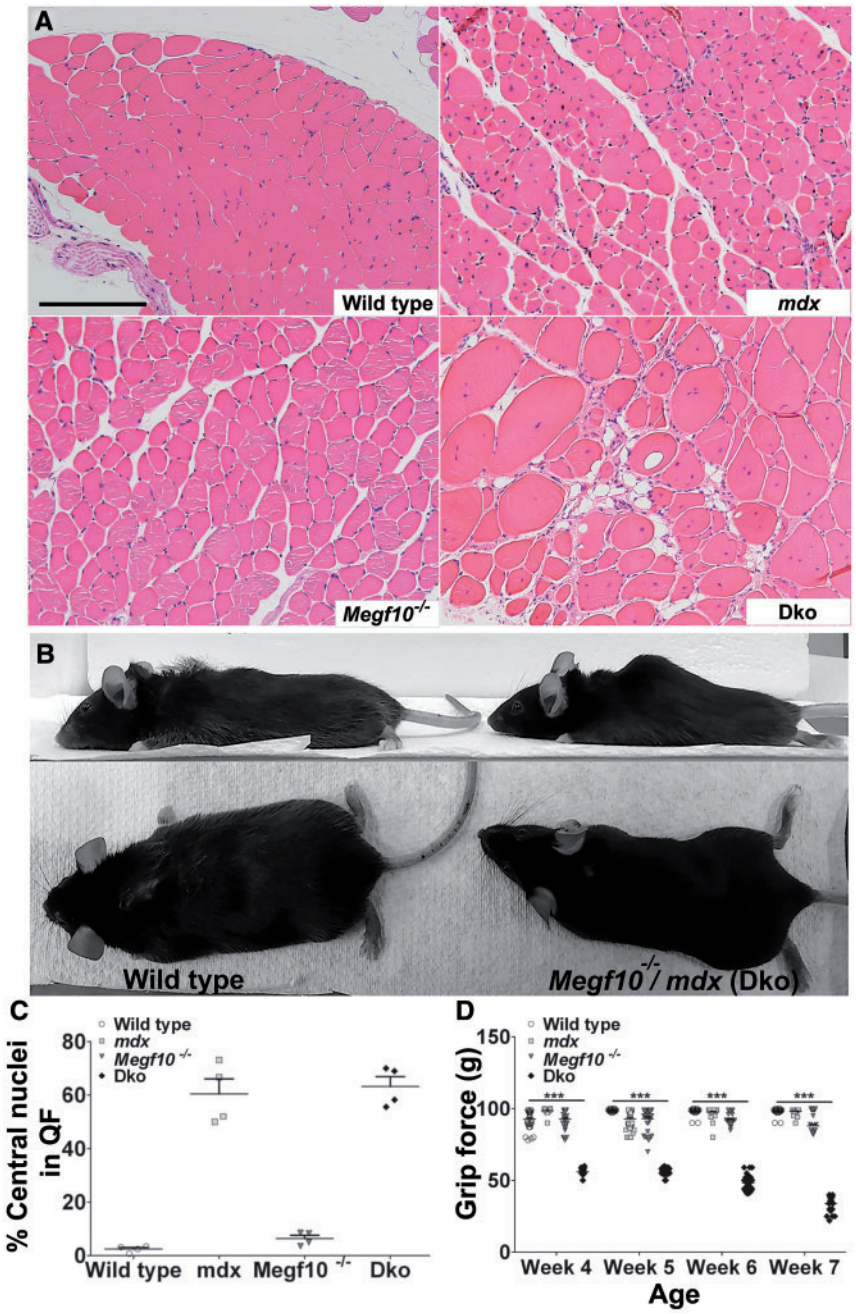

Figure 3. *Megf10*$^{-/-}$*/mdx* double knockout (dko) mice have a myopathic phenotype. Transverse sections of quadriceps femoris from two month old mice representing each genotype were stained with hematoxylin and eosin (**A**); scale bar, 50 μm. Photographs of representative wild type (left) and dko mice (right) at 2 months of age (**B**); note the dko mouse's kyphosis and slack posture. The proportions of centralized nuclei in *mdx* and dko mouse muscles are similar (**C**). Maximal forelimb grip strength was measured from wild type, *Megf10*$^{-/-}$, *mdx*, and dko mice; the ANOVA *P* value is < 0.0001 (**D**).

Fig. S13B). Notch1 localization to the nucleus is impaired in Megf10 shRNA-treated C2C12 cells (Fig. 9F and Supplementary Material, Fig. S13A).

Pathogenic p.C774R mutations that impair tyrosine phosphorylation of MEGF10 also impair binding of MEGF10 to Notch1

MEGF10 consists of 17 EGF-like domains in the ECD (amino acids 26-857), a transmembrane domain, and an ICD (amino acids 879-1140) composed of 13 tyrosine residues. Immunoprecipitation assays were performed with ICD deletion mutants of MEGF10. Deletion of the Y1016 to Y1099 amino acid residues of MEGF10 (Del2) resulted in complete loss of Notch1 binding whereas deletion of the Y879 to Y1002 amino acid residues of MEGF10 (Del1) was associated with only partial loss of Notch1 binding (Fig. 10A). Immunoprecipitation assays were performed on cell lysates from C2C12 cells transfected with p.Y1030F mutant Megf10 and a combined Y1016/1030/1061F mutant Megf10. These point mutations that disrupt tyrosine phosphorylation impaired Megf10 and Notch1 interactions (Fig. 10B). Furthermore, reduced binding of Notch1 to Megf10 was more prominent with transfection of

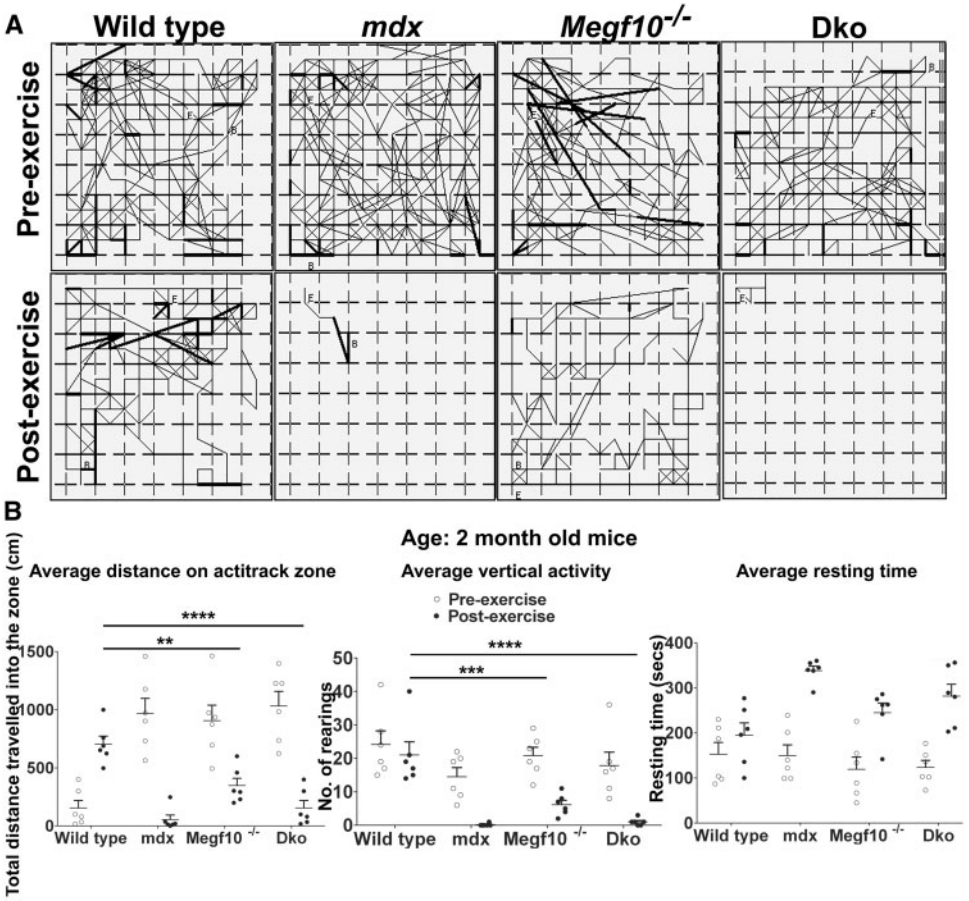

Figure 4. *Megf10*$^{-/-}$, *mdx*, and *Megf10*$^{-/-}$*/mdx* double knockout (dko) mice have decreased motor function. Representative ActiTrack activity plots of the 4 mouse genotype cohorts show activity levels before and after treadmill exercise ($n = 5$ for each cohort but the graph for one mouse is shown for each genotype). Thin lines represent distance traveled, while darker lines represent instances of vertical activity (rearing) and revisited routes (**A**). Graphs indicate average distances traveled (the ANOVA *P* value is 0.0003), average vertical activity (the ANOVA *P* value is < 0.0001), and average resting time of mice before and after treadmill exercise (the ANOVA *P* value is 0.0183) during ActiTrack testing (**B**). Post-test comparison results are indicated as follows: $^{**}P < 0.01$; $^{***}P < 0.001$, $^{****}P < 0.0001$.

p.C774R mutant MEGF10 compared to transfection of wildtype and p.C326R mutant MEGF10 (Fig. 10C). Immunofluorescence studies of C2C12 myoblasts transfected with p.C774R mutant MEGF10 showed no perceptible impairment of Notch1 localization to the nucleus (Fig. 10D), in contrast to the findings in shRNA Megf10 knockdown cells (Fig. 9F).

Blocking Notch1 activation with N-[N-(3,5-difluorophenacetyl-l-alanyl)]-S-phenylglycine t-butyl ester (DAPT) impairs cell viability in Megf10 shRNA knockdown myoblasts

Megf10 shRNA knockdown C2C12 cells, scrambled shRNA cells, and control cells were subjected to treatment with the γ-secretase inhibitor DAPT at 10 μM concentration for 48 h. Megf10 shRNA C2C12 myoblasts showed visibly reduced cell viability in response to DAPT treatment compared to scrambled shRNA and control myoblasts. In contrast, the Megf10 shRNA myoblasts did not show any morphological changes in vehicle (DMSO) alone (Supplementary Material, Fig. S14).

Discussion

The current study makes use of whole gene manipulations in myoblasts, modeling of known pathogenic mutations in myoblasts, and examination of mouse models to further characterize the cellular functions of MEGF10 in muscle, as well as its interactions with the Notch1 receptor and potential interactions with dystrophin. Our findings indicate that MEGF10 plays an important role in myoblast proliferation and migration, and that these functions may be compromised in the human muscle disease EMARDD. Megf10-deficient primary mouse myoblasts have distinct impairments in proliferation and migration that are more severe than those previously observed in *mdx* primary myoblasts (21). Furthermore, in the context of previous publications from our group (13) and others (2), our results indicate that the interactions between MEGF10 and Notch1 may be impaired in the human disease, and that the defect in tyrosine phosphorylation that has been associated with the human mutation p.C774R also impacts the interaction with Notch1. Nuclear localization of Notch1 in C2C12 cells appears to be impaired in Megf10 shRNA treated C2C12 cells, but not in p.C774R overexpressing C2C12 cells. The more severe effect of DAPT on cell viability, in contrast to the more targeted effect on cell proliferation with Notch1 shRNA knockdown, is likely due to the more global inhibition of the Notch signaling pathway induced by DAPT (22).

Nonsense mutations in *MEGF10* have been associated with EMARDD (8), thus whole gene knockdown in vitro and whole gene knockout in vivo are reasonable approaches to modeling

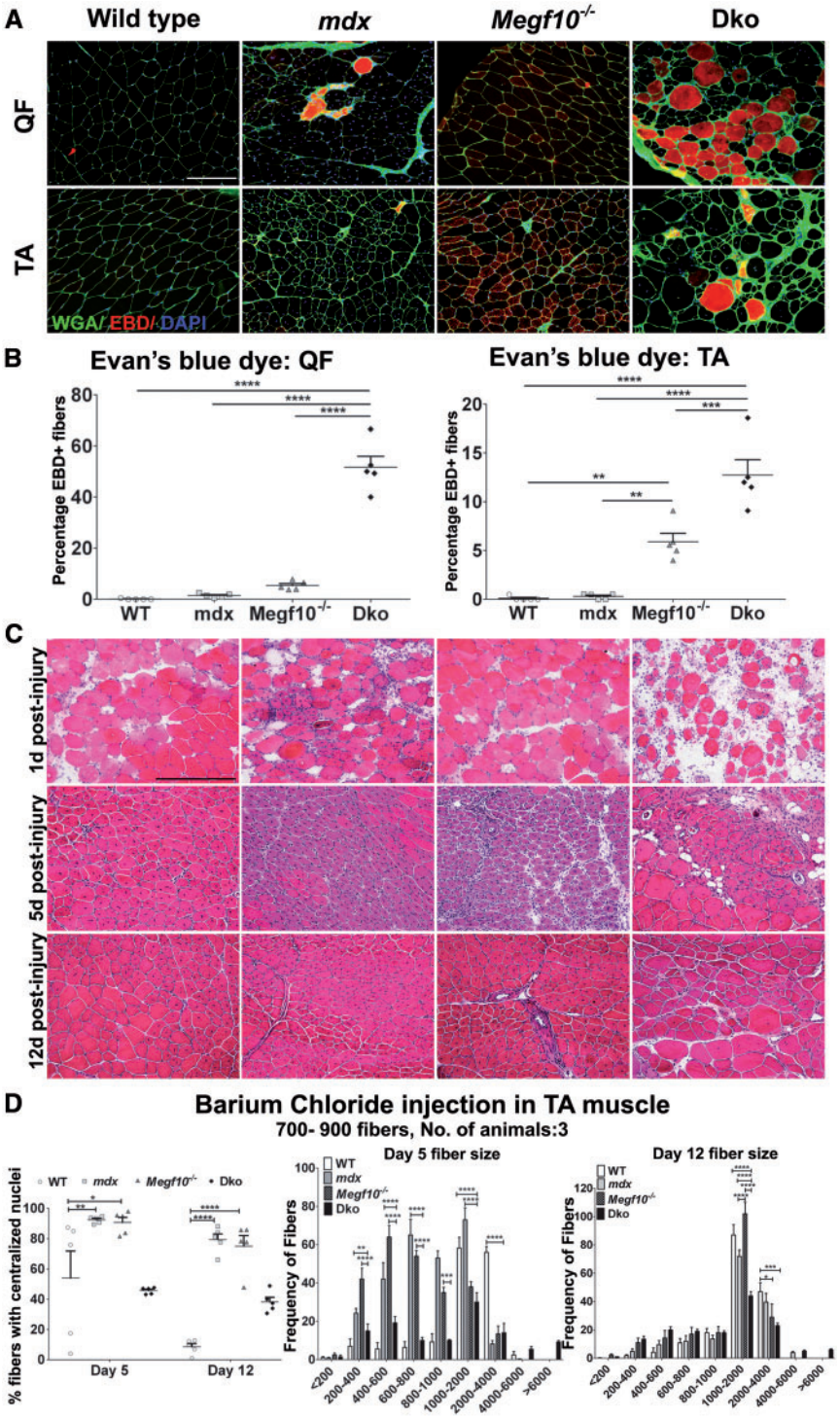

Figure 5. *Megf10*$^{-/-}$, *mdx*, and *Megf10*$^{-/-}$/ *mdx* double knockout (dko) mice display increased sarcolemmal permeability, endomysial fibrosis, and delayed regeneration. TA muscle sections representing the four mouse genotypes show Evans blue dye staining (red fluorescence) and wheat germ agglutinin-conjugated Alexa 488 (green fluorescence) to demarcate the myofiber basal lamina (**A**). Quantification of Evans blue dye positive fibers (**B**) in quadriceps femoris (left) and tibialis anterior (right) ($n = 3$ mice); ANOVA P values are <0.0001 for both graphs. Hematoxylin and eosin staining of TA muscles 1, 5, and 12 days after injection with 1.2% barium chloride (**C**). Analysis of muscle fibers after barium chloride injection (**D**) indicates quantification of centralized nuclei at day 5 and day 12 after injection in tibialis anterior muscles of three different mice for each genotype (left), along with the distributions of different fiber sizes in tibialis anterior at day 5 (middle) and day 12 (right). A range of 700–900 fibers were measured for each genotype in μm^2. The ANOVA P values for days 5 and 12 are each <0.0001. Scale bars, 20 μm. Post-test comparison results are indicated as follows: $^{*}P < 0.05$; $^{**}P < 0.01$; $^{***}P < 0.001$, $^{****}P < 0.0001$.

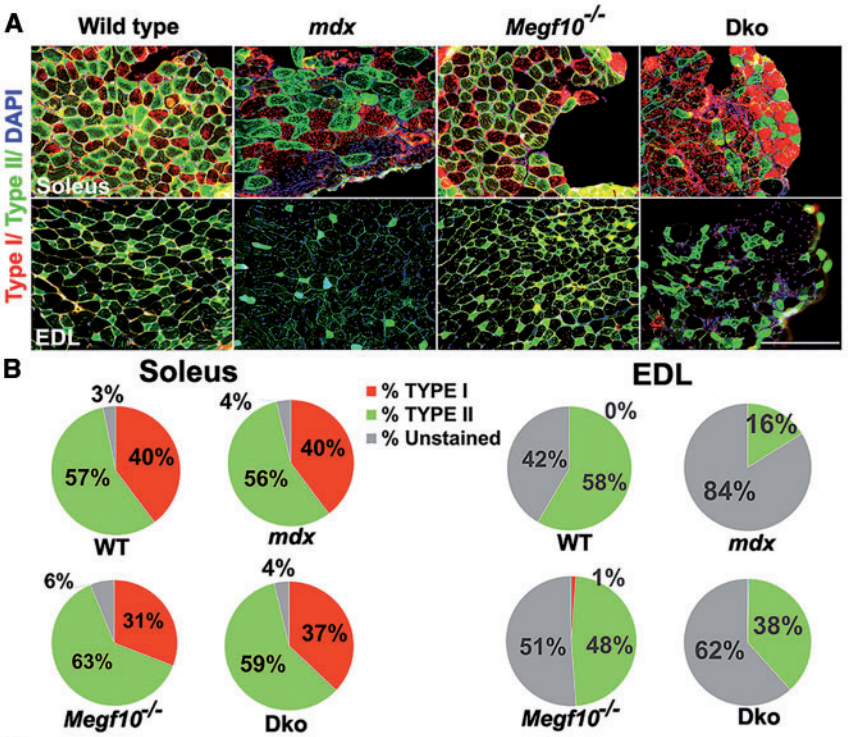

C

Table 1: Fiber size analysis (μm²)	Wild type		mdx		Megf10-/-		Dko	
	Soleus	EDL	Soleus	EDL	Soleus	EDL	Soleus	EDL
CSA	1996	2061	2772	1603	2190	1258	1675	1098
CSA Type I	1863	N/A	2651	N/A	2437	1433	1870	1393
CSA Type IIa	2118	1248	2837	1004	2044	895	1354	6664

Figure 6. *Megf10*$^{-/-}$ / *mdx* double knockout (dko) mouse muscles display skewed fiber type proportions. Representative images of myosin heavy chain type I (red), type IIa (green), and nuclei (blue) staining of serial sections in soleus and EDL of wild type, *mdx*, *Megf10*$^{-/-}$, and dko mice ($n = 3$ mice for each genotype) (**A**). The pie chart depicts the fiber type analysis of mouse muscles (**B**). The table shows cross-sectional fiber sizes of soleus and EDL from the four mouse strains (μm^2) (**C**).

the human disease. In addition, a mutation in the highly conserved extracellular cysteine residue at position 774 (8,9) is more damaging than a paired mutation in a different cysteine residue, p.C326 (13). The loss of critical cysteine residues can disrupt disulfide bonds, leading to improper folding and destabilization of proteins (23), sometimes with severe phenotypic consequences; an example is Walker–Warburg syndrome (24,25). Despite the extracellular location of the clinically relevant cysteine residues at positions 326 and 774 in MEGF10, mutations affecting these residues, especially p.C774R, impair tyrosine phosphorylation in the ICD, i.e., the phosphorylation of p.Y1030 (13). Impaired tyrosine phosphorylation at p.Y1030 is associated with reduced myoblast proliferation (13), and the homozygous p.Y1048X mutation has been associated with a severe form of EMARDD (8). Mutant overexpression has been used previously for this gene (14) as well as others representing recessive diseases (26).

We have found that Megf10 and Notch1 display similar patterns of expression in proliferating and differentiating myoblasts, and that Notch1 expression is reduced in Megf10-deficient mouse muscles, most prominently at the protein level. Notch1 contributes to both myoblast and satellite cell function (16). Activation of the Notch pathway helps maintain satellite cells in the quiescent state (27), contributes to their self-renewal (28), and contributes to their homing to target myofibers (16); such cellular functions may also be regulated by MEGF10. Notch1 interacts with Myf5 and Desmin during myoblast proliferation (29). During epithelial remodeling in *Drosophila* eyes, Notch1 regulates cell adhesion (30). Notch1 contributions to cell migration appear to be mediated by interactions with MKP-1 and antagonism of Mef-2 activity (31,32). Notch1 is activated for all of these cellular activities (29) and is inhibited during myoblast differentiation (33).

Unexpectedly, we found that Megf10 and Notch1 interact at their ICDs, though these proteins only seem to co-localize at the cell membrane, not the nucleus. Furthermore, we showed that (i) deletion of the Megf10 ICD, (ii) overexpression of p.C774R mutant MEGF10, which leads to decreased phosphorylation at the intracellular p.Y1030 tyrosine and (iii) direct impairment of tyrosine p.Y1030 phosphorylation (via a point mutation), all disrupt this interaction. Previous studies had indicated that members of the MEGF family of proteins might regulate Notch1 signaling. Structural similarity found between (i) canonical Notch1 ligands (e.g., Jagged-1, Delta), (ii) the EGF-like domains of Megf10, Megf11 and Megf12 (Jedi), and (iii) the delta/serrate/LAG-2 (DSL) motif required for canonical ligands to bind Notch1, suggested

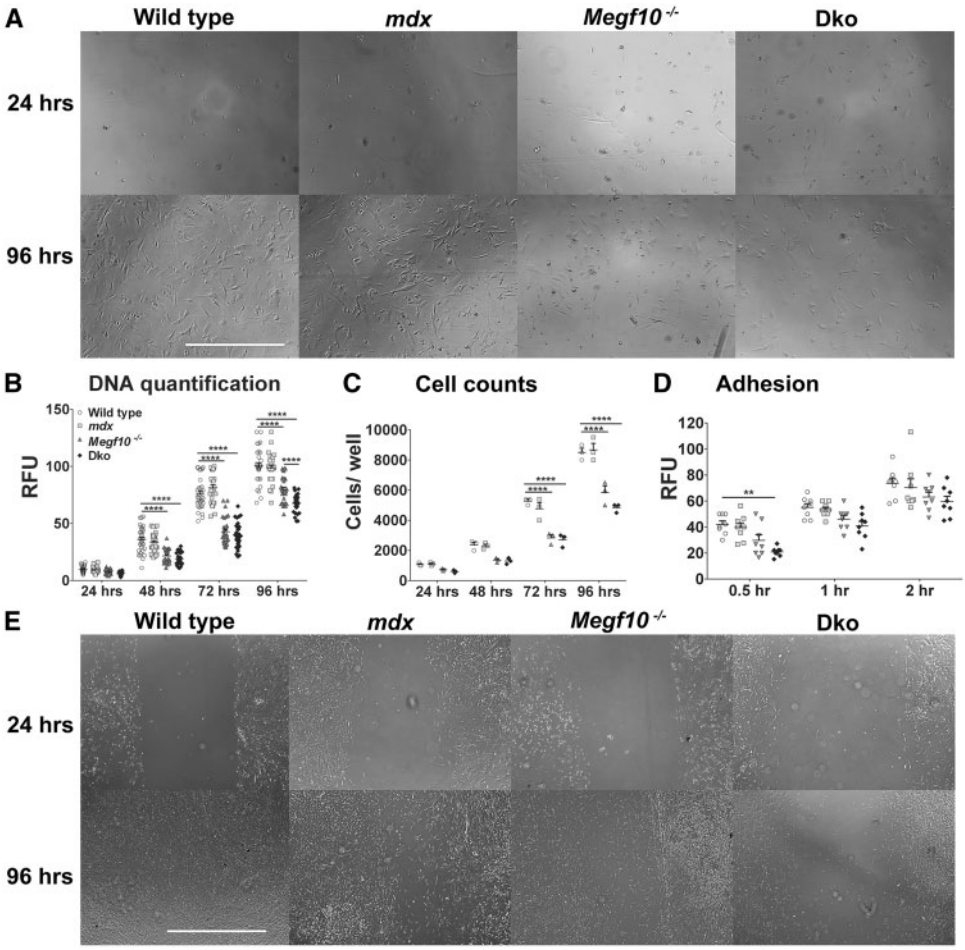

Figure 7. Primary myoblasts isolated from *Megf10*$^{-/-}$ and dko mice have impaired proliferation and migration compared to those from *mdx* and wild type mice. Photographs of wild type, *mdx*, *Megf10*$^{-/-}$, and dko primary myoblasts were taken 24 and 96 h after plating (**A**); scale bar, 2 mm. DNA quantification was performed using a CyQUANT kit, with scatter plots representing the mean absorbance ± S.E.M from $n = 24$ (**B**); the ANOVA *P* value is < 0.0001. Live cells were counted directly, with scatterplots representing the mean number of cells per well ± S.E.M from three independent experiments (**C**); the ANOVA *P* value is < 0.0001. Adhesion was assessed after the addition of calcein, with scatter plots representing the mean fluorescence ± S.E.M., $n = 8$ (**D**); the ANOVA *P* value was not statistically significant. Scratch zones were photographed at 24 and 96 h of culture after scratch with a 200 µl pipette tip (**E**). Post-test comparison results are indicated as follows: $^{**}P < 0.01$; $^{****}P < 0.0001$; RFU, relative fluorescence units; ns, not significant; scale bar, 5mm.

that these three peptides might act as Notch1 ligands (17). Notably, the ECD of Megf12 can inhibit Notch1 signaling in a manner comparable to that obtained with Jagged-1 (17). These studies also demonstrated that the ICD of Megf12, which is phosphorylated at conserved tyrosine residues (e.g., Y923, the equivalent of Megf10 Y1030), is essential to induce cellular functions such as inhibition of hematopoietic differentiation (17). Further highlighting the importance of conserved intracellular tyrosines in MEGF10 family members, the phosphorylation of Y949 within the immunoreceptor tyrosine-based activation motif (ITAM) domain of Drpr, the fly homolog of mammalian Megf10, is critical to cellular functions such as macrophage migration toward wounds (34). In addition, it was shown that Megf10 knockdown in myoblasts results in downregulation of Notch1, Notch3, and of the downstream effector of Notch1, HES-1 (2). Our findings provide complementary data documenting possible regulation of Notch1 by MEGF family members.

Canonical ligands of Notch1 may either activate or inhibit it, when expressed *in trans* (ligand based in a neighboring cell), or *in cis* (ligand based in the same cell) to the Notch1 receptor, respectively (35). The discovery of an expanding list of non-canonical, membrane-tethered ligands of Notch1 such as Delta-like 1 (Dlk-1) (36,37) and Delta/Notch1-like EGF-related receptor (DNER) (38) highlights the range of molecular processes that are able to fine tune this juxtacrine signaling pathway. Investigations focused on finding Notch1 modulators with therapeutic potential led to the identification of a 17 amino-acid peptide agonist derived from the Jagged-1 delta/serrate/LAG-2 (DSL) sequence (39,40). Few reports have documented modulation of Notch1 signaling via the ligand's ICD (Notch1 ligands' ICDs display the lowest level of conservation). However, the canonical form of delta-like 1 (Dll-1), expressed in cis to Notch1, plays a key regulatory function via its ICD, which binds to the Notch1 ICD in the nucleus, abolishing Notch1-regulated repression of MyoD activation (41). This finding agrees with a previous report showing that the recombinantly expressed soluble ICD of *Drosophila* Delta localizes to the cell nucleus (42). A restricted subpopulation of "committed" satellite cells that express Megf10 also express Dll-1 (2). It would be of interest to determine whether in committed satellite cells (which express MyoD) (43), Megf10 interacts with Notch1, Dll-1, or both.

We characterized a *Megf10*$^{-/-}$ mouse model whose ophthalmologic features have been extensively described, but not an

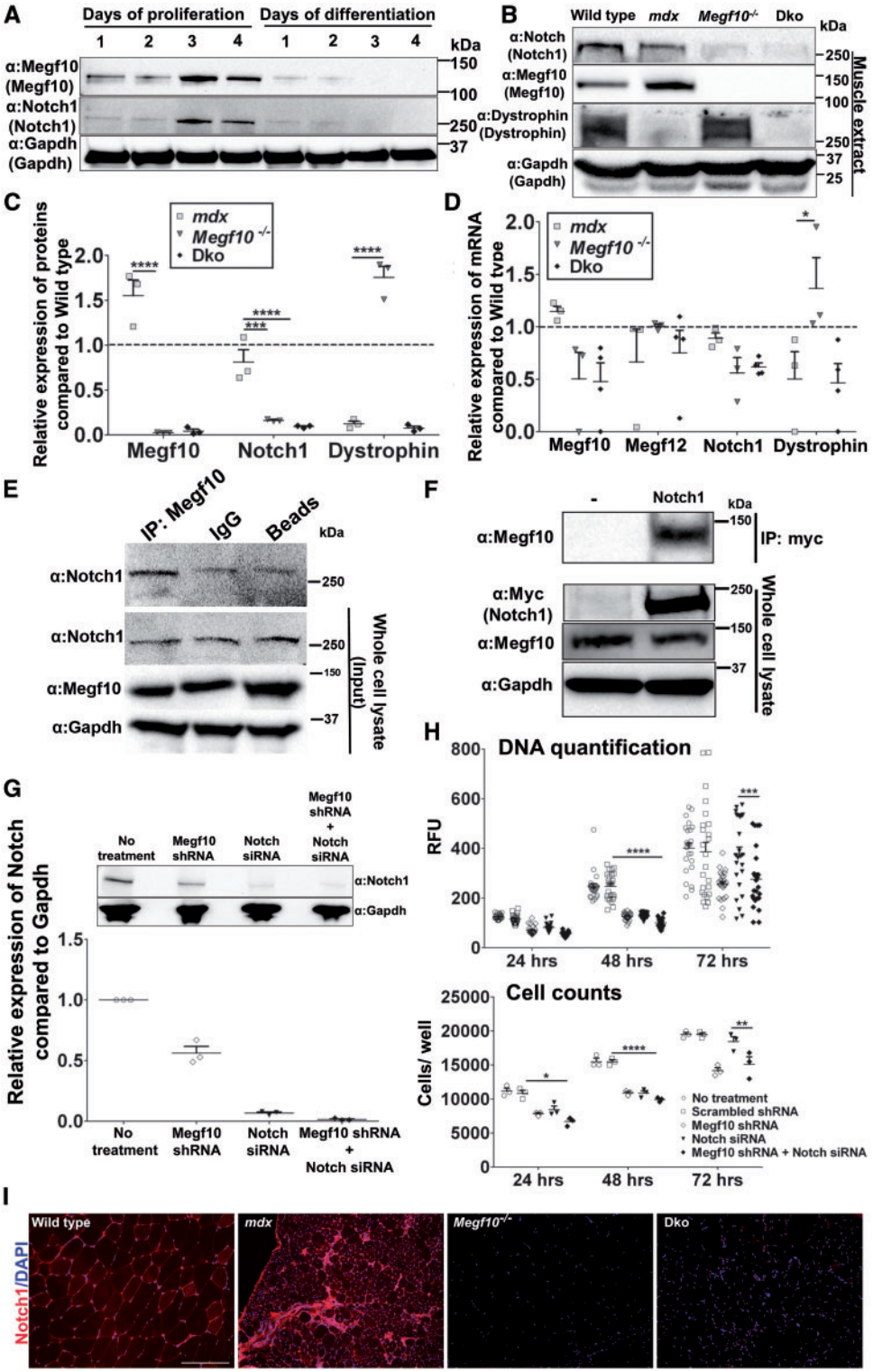

Figure 8. Megf10 interacts with Notch1. Megf10 and Notch1 expression levels were quantified in whole cell lysates of C2C12 cells via Western blot at the specified days of proliferation and differentiation after seeding (**A**). Western blot shows expression of Notch1, Megf10 and Dystrophin in quadriceps femoris muscle extracted from wild type, *mdx*, *Megf10*$^{-/-}$ and dko mice (**B**). The Western blot results were quantified via densitometric analysis, $n = 3$ (**C**); scatter plots represent the mean expression ± S.E.M from three independent experiments, with the ANOVA P value < 0.0001. RT-PCR expression analysis was performed on mRNA extracted from quadriceps femoris muscle representing wild type, *mdx*, *Megf10*$^{-/-}$ and dko mice. Data represent the mean ± S.E.M from at least three independent experiments, each done in triplicate (**D**). Expression ($2^{-\Delta\Delta CT}$) levels are shown relative to an 18S endogenous control; the ANOVA P value is 0.01. Whole cell lysates from C2C12 cells cultured for 72 h were subjected to immunoprecipitation with a Megf10 antibody. The immune complexes and whole cell lysates were then subjected to immunoblotting using a Notch1 antibody, with an IgG precipitation and beads serving as negative controls (**E**). The trace recovery of Notch1 with IgG precipitation is in line with control findings for other proteins in similarly structured experiments (57,58). Whole cell extracts of C2C12 cells were transfected with Myc-tagged Notch1 (the non-transfection control is indicated by the "-"). The immune complexes and whole cell lysates were subjected to immunoblotting with Megf10 and anti-Myc antibody (**F**). Simultaneous

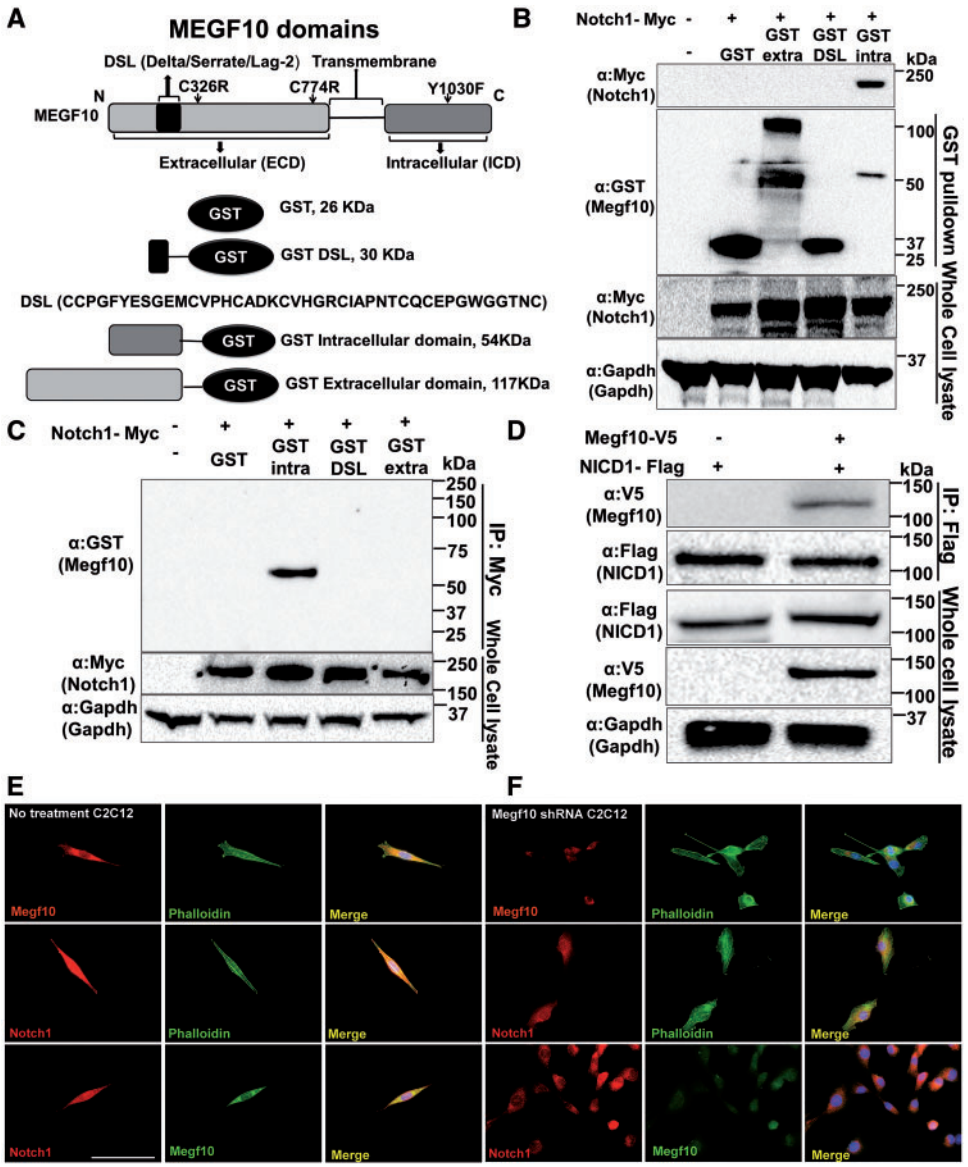

Figure 9. The ICD of MEGF10 interacts with Notch1. Diagram of GST-tagged domains of MEGF10 (**A**) show relevant missense mutations of MEGF10, including C326R, C774R, and Y1030F (the first two have been described in human disease, and the third is a mutation generated in vitro to represent defective tyrosine phosphorylation and has not been described in human disease to date). Glutathione-S-Transferase (GST) pulldown was performed using the extracellular, delta/serrate/LAG-2 (DSL) and intracellular domains of MEGF10 after successful co-transfection of GST-tagged Megf10 domains and Myc-Notch1 into C2C12 myoblasts (**B**). Reciprocal experiments were performed by immunoprecipitating myc-Notch1 and then immunoblotting with GST antibody (**C**). V5-tagged wild type MEGF10 and Flag-NICD1 were each co-transfected into C2C12 cells, followed by co-immunoprecipitation of cell lysates with anti-flag antibody, and then immunoblotting with anti V5-antibody, along with appropriate control antibodies (**D**). Gapdh was used as a loading control for all Western blots. Immunofluorescence of untreated wild type C2C12 cells with antibodies to Megf10, Notch1 and Phalloidin shows that Megf10 and Notch1 mainly co-localize at the cell membrane (**E**). Notch1 expression is low for Megf10 shRNA treated C2C12 cells (**F**) visualized at 40X magnification; scale bar, 20μm.

analysis of its muscle structure and function (3). Animal models of Megf10 deficiency were previously created and/or characterized in zebrafish (i.e., shRNA-mediated knockdown) (9) and *Drosophila* (i.e. *drpr* null mutant flies) (15). However, a mammalian model that recapitulates aspects of the muscle phenotype observed in patients (8,9) has not previously been described. Our data indicate that dystrophin expression is increased in the muscle tissue of *Megf10*$^{-/-}$ mice, suggesting a possible interaction between the two proteins. Furthermore, a recent study indicates that dystrophin plays an important role in satellite cell

knockdown of Megf10 and Notch1 was performed in C2C12 myoblasts that was quantified on scatterplot (**G**) with an ANOVA *P* value < 0.0001, confirmed on Western blot (top) that was quantified via densitometry analysis from three independent experiments (bottom). C2C12 myoblast proliferation was quantified at 24, 48, and 72 h after simultaneous knockdown of Notch1 and Megf10 (**H**). DNA quantification was performed using a CyQUANT kit, with scatter plots representing the mean absorbance ± S.E.M from $n = 24$ (top); the ANOVA *P* value is < 0.0001. Live cells were also counted directly, with scatter plots representing the mean number of cells per well ± S.E.M from three independent experiments (bottom); the ANOVA *P* value is < 0.0001. Post-test comparison results are indicated as follows: $^{*}P < 0.05$; $^{**}P < 0.01$; $^{***}P < 0.001$; RFU, relative fluorescence units; ns, not significant. Gapdh served as the loading control throughout. Representative images of Notch1 (blue) and nuclei (blue) staining of serial sections obtained from quadriceps femoris of wild type, *mdx*, *Megf10*$^{-/-}$, and dko mice (**I**). Muscle samples from 3 mice were examined for each strain.

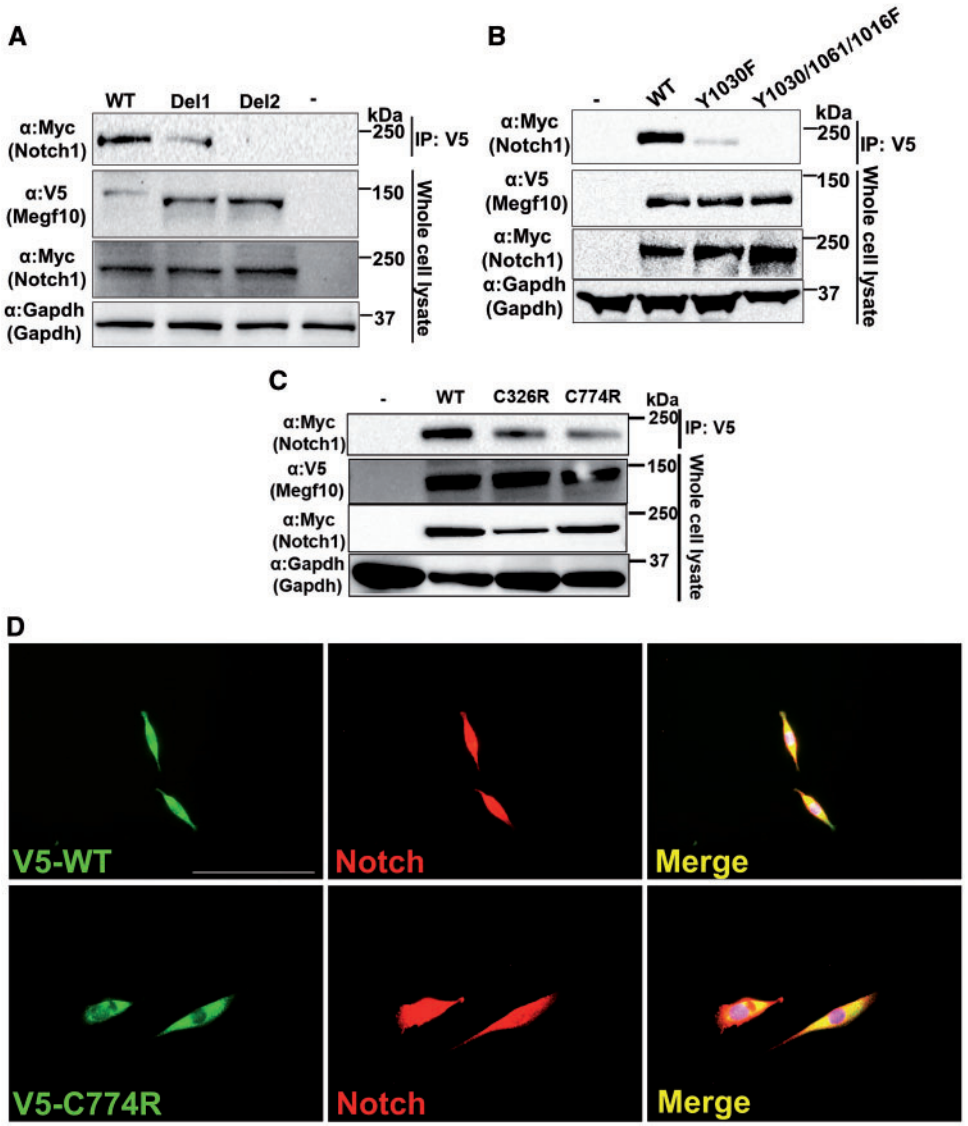

Figure 10. MEGF10 mutations impair interactions with Notch1. V5-tagged human MEGF10 containing two different intracellular deletion mutations (Del1, deletion from Y879 to Y1002 and Del2, deletion from Y1016 to Y1099) were each co-transfected with myc-tagged Notch1 into C2C12 cells (**A**). V5-tagged MEGF10 containing intracellular point mutations were each co-transfected with myc-tagged Notch1 into C2C12 cells (**B**). V5-tagged MEGF10 containing extracellular domain disease-causing p.C774R and p.C326R point mutations were each co-transfected with myc-tagged Notch1 into C2C12 cells (**C**). For each experiment, co-immunoprecipitation was performed on cell lysates with anti-V5 antibody, then the immune complexes were immunoblotted with anti-myc antibody. Gapdh was used as a loading control throughout. Immunofluorescence of V5-tagged WT and p.C774R MEGF10 transfected C2C12 cells with antibodies to V5 and Notch1 show co-localization of Megf10 and Notch1 at the cell membrane, along with localization of Notch1 only at the nucleus (**D**), as seen in wild type C2C12 cells (Fig. 9E); scale bar, 20 μm.

polarity and asymmetrical division (44), while another found evidence for interactions between dystrophin and the Notch signaling pathway (45). The dko mouse had clear abnormalities on grip force testing and histological analysis at rest that contrasted with findings in the single knockout mouse. However, the *Megf10*$^{-/-}$ mouse, *mdx* mouse, and dko mouse all showed delayed histological responses to injury, and primary myoblasts isolated from each of these three strains displayed comparable defects in proliferation and migration. It is possible that in rodents, the Megf10 paralogs Megf11 and/or Megf12 compensate for the loss of Megf10. The fly model of Megf10 myopathy displays marked muscle histological abnormalities (15). *Mdx* mice also display mild muscle weakness, but in contrast to *Megf10*$^{-/-}$ mice show consistent, albeit moderately severe, skeletal muscle histological abnormalities, and are thus frequently used to model Duchene muscular dystrophy (46–48).

Our results suggest several directions for future study. The implications of the interaction between MEGF10 and Notch1 merit further exploration in multiple contexts relevant to myogenesis, in both myoblast cultures and animal models. Elucidation of more details of this interaction may also help explain the role of tyrosine phosphorylation in the function of MEGF10. Given the presence of a small amount of endogenous wild type Megf10 in transfected C2C12 cells, the development of a CRISPR-Cas9 model would help confirm and extend findings from the current study. Given the known functions of MEGF10 in the central nervous system (6), an examination of potential peripheral nerve pathology may be

worthwhile, but the published reports on human subjects with EMARDD do not indicate a neurogenic component to this disease (8–12).

The disease mechanism of EMARDD thus may be quite complex, involving defects in tyrosine phosphorylation that in turn may impair the interactions between Megf10 and Notch1. The parallel yet not identical functional defects caused by Megf10 deficiency and the p.C774R mutation in that gene are instructive, and bear further investigation in the setting of the Notch1 pathway interactions. Such studies could lead to new approaches to manipulate myoblasts and satellite cells for potential therapeutic applications not only for EMARDD but also other muscle diseases.

Materials and Methods

Cell culture

C2C12 myoblasts (American Type Culture Collection) were cultured in Dulbecco's modified Eagle's medium (DMEM, Life Technologies) with 20% fetal bovine serum (Sigma), penicillin (50 units/ml), and streptomycin (50 μg/ml) (Invitrogen). At 90% confluence, the growth medium was replaced with low-serum differentiation medium (2% equine serum in DMEM) containing antibiotics. Differentiation medium was replenished daily for 4 days (49).

shRNA knockdown and overexpression via transfection

A cocktail of three *Megf10* short hairpin RNAs (shRNAs) GTTGTACTTGCACCAACA, CCAACAGGAATGTCTATGA, GCACC ACTTGCCAGAGAAT, inserted into a pZIP vector containing *GFP* (GE Healthcare Dharmacon), was transfected into C2C12 cells that had been plated in medium without antibiotics. Scrambled shRNA was transfected into separate cultures as a control. GFP expression was monitored for 48 h after transfection to determine transgene expression. Selected colonies displaying GFP expression were grown in media containing puromycin (4 μg/ml) according to a puromycin death curve generated for C2C12 myoblasts. Previously described V5-tagged human wild type, p.C774R mutant, and p.C326R mutant *MEGF10*, and empty pCS2 vectors (13) were transfected into C2C12 cells using Lipofectamine 3000 (Life Technologies Corporation). Previously described p.Y1016F, p.Y1030D, p.Y1030F, Y1061F, and deletion mutant *MEGF10* constructs (13) were also transfected into C2C12 cells. V5-tagged human wild type, p.C774R mutant, and p.C326R mutant *MEGF10* were analyzed by fluorescence-activated cell sorting (FACS). To detect V5 tagged MEGF10, transfected and untransfected cells were incubated with Alexa 488-conjugated (Zenon antibody labelling kits) antibodies to V5 (R960-25) (Thermofisher Scientific). Cells were analyzed in a FACS Calibur Flow Cytometer (BD Biosciences) at the University of Florida Interdisciplinary Center for Biotechnology Research (UF ICBR) Flow Cytometry Core Facility. N-[N-(3,5-difluorophenacetyl-l-alanyl)]-S-phenylglycine t-butyl ester (DAPT) and sterile DMSO were purchased from Sigma Aldrich and DAPT was diluted in 100% DMSO at 10μM. DAPT blocks the cleavage of Notch1, thus inhibiting Notch1 activation. The 10μM concentration was selected as it is ideal for blocking Notch1 cleavage in C2C12 cells without triggering cytotoxicity (50). Megf10 shRNA myoblasts, scrambled shRNA myoblasts, and untransfected controls were treated with diluted DAPT and DMSO vehicle.

RNA isolation and real-time PCR

Total RNA was isolated from C2C12 cells and muscle tissue (quadriceps femoris), and cDNA was generated using the cells-to-cDNA kit, RNAqueous-4PCR kit (Ambion, Thermo Fisher Scientific) and high capacity RNA to cDNA kit (Applied Biosystems). RT-PCR of cDNA was performed using the TaqMan Gene Expression Master Mix and TaqMan primer probe sets designed for Megf10, Megf12, Notch1, Dystrophin, Gapdh, and 18S (Thermo Fisher Scientific). Transcript levels were normalized to Gapdh and 18S transcript levels using the ΔΔCT method (51). ShRNA knockdown of Megf10 in C2C12 myoblasts was confirmed by RT-PCR (data not shown).

Primary myoblast culture

Primary myoblasts were isolated from hind limb muscles of neonatal mice using a skeletal muscle dissociation kit (Miltenyi Biotech) and cultured in Ham's F10 nutrient medium (Life Technologies) with 20% fetal bovine serum (Sigma), penicillin (50 units/ml), streptomycin (50 μg/ml), and fibroblast growth factor (Promega) (52).

Cell proliferation determination via manual cell counts and CyQUANT assays

To perform a manual cell count, cells were transfected, suspended in DMEM, mixed 1:1 with a 0.4% solution of Trypan Blue stain, and visualized and counted manually under a microscope using a hemocytometer. For the CyQUANT DNA quantification assay, stable shRNA treated and V5-transfected C2C12 myoblasts were re-plated at 5,000 cells/well in 96-well plates with 100 μL of 1X CyQUANT dye solution (Life Technologies) added to each well. Fluorescence was measured using a microplate reader (BioRad Laboratories) with excitation at 485 ± 10 nm and emission detection at 530 ± 12.5 nm.

TUNEL assay

TUNEL assay was performed using the Click-iT TUNEL Alexa Fluor 594 Imaging Assay (C10246; Invitrogen). Normal and shRNA-treated C2C12 myoblasts were plated onto 0.1% gelatin-coated coverslips. After 2 days, the cells were fixed with 4% paraformaldehyde for 1h at 4 °C. Staining for apoptotic cells was conducted according to the manufacturer's protocol. DNase-I treated cells were used as positive controls.

Cell adhesion assays

Cell adhesion assays were performed with the Vybranto Cell Adhesion Assay Kit (Life Technologies). Ninety-six-well plates were coated with fibronectin (Sigma, F0556) at 10 μg/ml. C2C12 cells treated with shRNA, C2C12 cells transfected with V5-tagged MEGF10 constructs, and primary mouse myoblasts were labeled with calcein AM. The fluorescence of adherent cells was measured at absorbance 494 nm ± 10 nm and emission of 517 nm ± 10 nm, and quantified by:

$$\mathrm{RFU} = \frac{\mathrm{Fluorescence}_{\mathrm{adherent\ cells}}}{\mathrm{Fluorescence}_{\mathrm{total}}} \times 100$$

Cell migration assays

Cell migration was assessed as previously described with minor modifications (53). C2C12 cells treated with shRNA and C2C12 cells transfected with V5-tagged MEGF10 plasmids were seeded in 6 cm dishes at $1.5x10^5$ cells/dish. Primary myoblasts were seeded in 6-well plates at 50,000 cells/well. Cells were grown to 99% confluence, and then scratched with a 200 μl pipette tip to create a linear cell-free zone. The cell debris was immediately washed off. Defined areas of the cell free zone were visualized at 4X magnification using a phase contrast microscope at 0, 24, 48, and 72 h. Primary myoblasts were also imaged at 96 h due to their slower growth rate.

Mouse strains

Wild type C57BL/6J mice were provided by Animal Care Services at the University of Florida. C57BL/10ScSn-*Dmd*^{mdx}/J mice (*mdx* mice) were purchased from the Jackson Laboratory (54). *Megf10*$^{+/-}$ mice on a C57BL/6 background were shared by Jeremy Kay and Joshua Sanes (3), and were bred to produce homozygous *Megf10*$^{-/-}$ mice. The *mdx* and *Megf10*$^{+/-}$ mice were subsequently bred to produce a *Megf10*$^{-/-}$/*mdx* double knockout (dko) strain. Genomic DNA was isolated from tail biopsies using the REDExtract-N-Amp Tissue PCR Kit (Sigma Aldrich). *Megf10* deletions were identified using the following PCR primers: 5' CTATGGAGTGAGTGTGATACCTGC 3' (forward, wild- type), 5' CCAACTGACCTTGGGCAAGAACAT 3' (reverse, wild-type), and 5' CCGGTAGCTGATTCTGTTTGAAGG 3' (reverse, mutant) (3). Expected amplicon sizes were 422 bp for the mutant allele and 656 bp for the wild type allele. The *Dmd* mutation in the *mdx* mouse was confirmed by amplifying exon 23 with the following PCR primers: 5' ATTTTGAGGCTCTGCAAAGTTC 3' (forward) and 5'GCCCCTCAATCTCTTCAAATTC 3' (reverse) (19). Amplified DNA fragments were sequenced at the DNA Sequencing Core Laboratory of the UF ICBR.

Force mechanics

After euthanasia, soleus and extensor digitorum longus (EDL) muscles were isolated from mice representing all four strains with the tendons attached, then suspended vertically in a water-jacketed bath containing Krebs–Henseleit solution equilibrated with a 95% O_2/5% CO_2 gas mixture and maintained at 37 °C. Muscles were stimulated using two vertical platinum electrodes. All contractile properties were measured isometrically following determination of optimum length. Peak isometric tetanic force was measured at 160Hz using a 500-msec train with a 2-min recovery period. Further, a force frequency relationship was determined by stimulating the muscle to contract using a 500-msec train with a 2-min recovery period at the following frequencies: 15Hz, 30Hz, 60Hz, 100Hz, 160Hz, and 200Hz. The equipment used for these experiments included a Grass AC/DC Strain Gage Amplifier (model P122) (Natus Medical Inc., Pleasonton, California), Aurora Scientific Signal Interface (Aurora Scientific Inc., Ontario, Canada), Grass S48 Stimulator, and Grass Force Displacement Transducer (model FT03).

Muscle functional testing, Evans blue dye injections, and barium chloride injections

Forelimb strength was measured using a grip strength apparatus (Columbus Instruments, Columbus, Ohio). Each mouse was held by the base of its tail and allowed to grasp the mesh monitor. The mouse was then gradually drawn away until it released the mesh. The force at release was recorded. This was repeated five additional times within 10 min for each mouse. Data are presented as mean ± standard error of the mean. For ActiTrack analysis (Harvard Apparatus, Holliston, Massachusetts), 6-min activity assays were performed as previously described (55), with each of the four genotypes represented by five mice at two months of age. Pre- and post-treadmill activity (total distance and vertical activity) were measured for 6 min using ActiTrack v2.7 software (Panlab). For treadmill exercise, the mice were run for 5 min at three meters/min, followed by an increase to ten meters/min for 10 min. For Evans blue dye (EBD) studies, two-month-old mice underwent intraperitoneal injections of 10μg/μl Evan's blue dye in sterile PBS solution. The mice were euthanized 24 h after injection, and skeletal muscle tissue was harvested. For the barium chloride studies, 2-month-old mice were injected with 50 μl of 1.2% barium chloride in sterile water in the TA muscle of the right hind limb. The contralateral TA muscle was injected with 50 μl of sterile water. TA muscles were harvested 1, 5, and 12 days after injury.

Muscle histology

Quadriceps femoris, gastrocnemius, and tibialis anterior muscle samples were extracted post-mortem from all four strains of mice, embedded in paraffin or snap frozen, sectioned at 5 μm, then fixed onto slides in the Pathology Core at the University of Florida. Samples were incubated for 5 min in hematoxylin (Leica Biosystems); rinsed with cold tap water; immersed twice in eosin Y; washed with 80, 90, and 100% ethanol; and incubated three times for 2 min in xylene. The samples were mounted with Cytoseal 60 (Richard Allan Scientific) and visualized on an Olympus BX43 upright microscope. Central nucleation was calculated by counting centralized nuclei per section and dividing by the total number of nuclei per section.

Immunohistochemical studies

Snap frozen muscle sections from mice injected with Evans blue dye were co-stained with wheat germ agglutinin (WGA) conjugated with Alexa-488 (Thermofisher) and DAPI (40 6-diamidino-2-phenylindole). Confocal images were visualized on an Olympus BX43 upright microscope. Fiber typing analysis was done with snap frozen muscle tissue (soleii and EDL) which were co-stained with MHC Type I A4.840 (MYH7) (Developmental Studies Hybridoma Bank, IgM) and MHC Type IIa SC-71 (MYH2) (Developmental Studies Hybridoma Bank, IgG). Secondary antibodies Alexa 568 (IgM, Type I) and Alexa 488 (IgG, Type II) (ThermoFisher Scientific) were used to visualize fiber types. Cross-sectional areas were measured in at least five to seven sections of muscle tissue from each strain using Image J software. Quadriceps femoris muscle was stained with anti-dystrophin (Novocastra), anti-utrophin (Novocastra), anti-Notch1 (DHSB), anti-Megf10 (Millipore) and DAPI.

Immunofluorescence and co-localization studies

C2C12 cells were cultured sparsely on coverslips, washed with PBS, fixed in 4% paraformaldehyde, then permeabilized with 0.1% Triton X-100 in PBS. After blocking with 10% fetal bovine serum in PBS, the cells were incubated with primary anti-Megf10 and anti-Notch1 antibodies (Developmental Studies Hybridoma Bank), then with Alexa-568 or Alexa-488 conjugated

goat anti-rabbit antibody, along with Alexa-568 goat anti-rat antibody mixed with anti-phalloidin antibody (Alexa-488) (Life Technologies). Coverslips were mounted with DAPI. Confocal images were visualized on an Olympus BX43 upright microscope. The myoblast fusion index was calculated as the ratio of the number of nuclei inside myotubes compared to the total number of nuclei × 100 at day 10 of myogenic differentiation via ImageJ software. Co-localization was quantified with the Coloc2 plugin for the ImageJ software program (https://imagej.net/Colocalization_Analysis) by calculating Manders split coefficients and Pearson's correlation coefficients for Megf10 (green) and Notch1 (red). Data are shown as mean ± S.E.M. (56)

Protein extraction from C2C12 cells and western blot studies

Forty-eight hours after transfection, C2C12 cells were lysed in RIPA buffer. Protein was extracted and quantified as described above. Western blots verified shRNA knockdown and overexpression of V5 constructs in transfected C2C12 cells (Supplementary Materials, Figs S1 and S2). Proteins were resolved on a 4–12% SDS-polyacrylamide gel (Life Technologies) and transferred onto a nitrocellulose membrane. The membrane was probed with antibodies to V5 at a 1:1000 dilution (Life Technologies), Megf10 at a 1:1000 dilution, Myc at a 1:1000 dilution (Life Technologies), GST at a 1:1000 dilution (Cell Signaling Technologies), Gapdh at a 1:1000 dilution, and β-actin at a 1:500 dilution (Santa Cruz).

Immunoblot studies from mouse muscle

Quadriceps femoris muscles were isolated from mice and subjected to mincing with a scalpel in RIPA buffer (25 mM Tris-HCl pH 7.6, 150 mM NaCl, 1% NP-40, 1% sodium deoxycholate, 0.1% SDS, 1 mM phenylmethylsulfonyl fluoride, 50 mM NaF, 1 mM Na_3VO_4). The minced muscle was transferred into prefilled tube kits containing 1 mm glass beads (Benchmark Scientific) for homogenization in a FastPrep homogenizer (Thermo Scientific). Cell lysate was spun at 14,000 *g* at 4 °C for 20 min. The total protein content of the supernatant was measured (BCA, Sigma), and 50 μg of the extract was resolved on a 4–12% SDS-polyacrylamide gel (Life Technologies), then transferred onto a nitrocellulose membrane (20 μm). The membrane was blocked in 5% milk/TBST (0.5% Tween-20, 8 mM Tris-Base, 25 mM Tris-HCL, 154 mM NaCl), then probed with antibodies to Notch1 (bTAN-20, Developmental Studies Hybridoma Bank), Megf10 (EMD Millipore), dystrophin 6-10E (a gift from Louis M. Kunkel), and Gapdh (Cell Signaling Technologies). The membrane was incubated with horseradish peroxidase-conjugated secondary antibodies and visualized by chemiluminescence (Thermo Scientific).

Co-immunoprecipitation studies with C2C12 cell lysates

Megf10 was immunoprecipitated using an anti-Megf10 antibody and protein A beads (Cell Signaling Technology). IgG solution was used as a negative control (Santa Cruz Biotechnology). Immune complexes were blotted with anti-Notch1 antibody. Myc-tagged Notch1, flag-tagged NICD1 (Notch1 ICD) (Addgene) and V5-tagged MEGf10 were transfected into C2C12 cells and later immunoprecipitated using anti-Myc antibody (Life Technologies), anti-flag antibody (Sigma), and anti-V5 (Life Technologies) from whole cell lysate. Proteins were resolved on a 4–12% SDS-polyacrylamide gel (Life Technologies) and transferred onto a nitrocellulose membrane that was then was probed with appropriate antibodies.

Cloning of MEGF10 domains and GST interaction assays

The delta/serrate/LAG-2 (DSL) domain, ECD, and ICD of *MEGF10* were amplified by PCR from full-length human *MEGF10* cDNA (pCS2-V5 HMEGF10) (13), encoding amino acids 146 to 187 (delta/serrate/LAG-2 (DSL) domain), 1 to 857 (ECD), and 879 to 1140 (ICD). Each PCR product was cloned into the pEBG GST fusion vector (Addgene), in-frame with the GST tag, and sequenced to confirm successful and correct cloning. GST interaction assays were performed with whole-cell extracts from transfected C2C12 cells that were pre-bound with glutathione resin. After incubation with the whole-cell extracts, glutathione bead-GST fusion protein complexes were collected by centrifugation, washed, then resuspended in sodium dodecyl sulfate loading buffer and boiled, followed by Western blotting.

Statistics

All data were expressed as mean ± SEM. Statistical analyses were performed using GraphPad Prism 5 (GraphPad Software). One-way ANOVA, followed by Bonferroni post hoc test, was used to analyze differences of myotube fusion index between groups. For other analyses, two-way ANOVA of repeated measurements was applied, followed by Bonferroni post hoc test. A p value <0.05 was considered statistically significant.

Study approval

Generation of plasmid constructs was conducted under the auspices of the Biosafety Program at the University of Florida. Mouse husbandry and breeding were conducted under the auspices of Animal Care Services at the University of Florida and Boston Children's Hospital, following protocols approved by the Institutional Animal Care and Use Committees (IACUC) at the University of Florida and Boston Children's Hospital.

Supplementary Material

Supplementary Material is available at *HMG* online.

Acknowledgements

The authors thank Jeremy N. Kay and Joshua Sanes for sharing the *Megf10*$^{-/-}$ mouse line, Yuanjing Liu and Laura Ranum for sharing the grip-strength device used in this study, Amy Donate for helpful discussions, Marda Jorgensen for guidance regarding immunostaining and Matthew Alexander for guidance regarding cell culture techniques.

Conflict of Interest statement. MS, ID, and PBK are using some of the functional assays described in the manuscript for a separate project that is supported by National Institute of Arthritis and Musculoskeletal and Skin Diseases (NIH) grant number R41AR068158. There are no other relevant financial interests.

Funding

National Institute of Neurological Disorders and Stroke (NINDS), National Institutes of Health (NIH) grant number R01 NS080929 (HMR, ID, and PBK), Department of Pediatrics at the University of Florida College of Medicine (MS and PBK), and the Ferlita Family Fund.

References

1. Chung, W.-S., Clarke, L.E., Wang, G.X., Stafford, B.K., Sher, A., Chakraborty, C., Joung, J., Foo, L.C., Thompson, A., Chen, C. *et al*. (2013) Astrocytes mediate synapse elimination through MEGF10 and MERTK pathways. *Nature*, **504**, 394–400.
2. Holterman, C.E., Le Grand, F., Kuang, S., Seale, P. and Rudnicki, M.A. (2007) Megf10 regulates the progression of the satellite cell myogenic program. *J. Cell Biol.*, **179**, 911–922.
3. Kay, J.N., Chu, M.W. and Sanes, J.R. (2012) MEGF10 and MEGF11 mediate homotypic interactions required for mosaic spacing of retinal neurons. *Nature*, **483**, 465–469.
4. Suzuki, E. and Nakayama, M. (2007) The mammalian Ced-1 ortholog MEGF10/KIAA1780 displays a novel adhesion pattern. *Exp. Cell Res.*, **313**, 2451–2464.
5. Ziegenfuss, J.S., Biswas, R., Avery, M.A., Hong, K., Sheehan, A.E., Yeung, Y.-G., Stanley, E.R. and Freeman, M.R. (2008) Draper-dependent glial phagocytic activity is mediated by Src and Syk family kinase signalling. *Nature*, **453**, 935–939.
6. Wu, H.H., Bellmunt, E., Scheib, J.L., Venegas, V., Burkert, C., Reichardt, L.F., Zhou, Z., Farinas, I. and Carter, B.D. (2009) Glial precursors clear sensory neuron corpses during development via Jedi-1, an engulfment receptor. *Nat. Neurosci.*, **12**, 1534–1541.
7. Suzuki, E. and Nakayama, M. (2007) MEGF10 is a mammalian ortholog of CED-1 that interacts with clathrin assembly protein complex 2 medium chain and induces large vacuole formation. *Exp. Cell Res.*, **313**, 3729–3742.
8. Logan, C.V., Lucke, B., Pottinger, C., Abdelhamed, Z.A., Parry, D.A., Szymanska, K., Diggle, C.P., van Riesen, A., Morgan, J.E., Markham, G. *et al*. (2011) Mutations in MEGF10, a regulator of satellite cell myogenesis, cause early onset myopathy, areflexia, respiratory distress and dysphagia (EMARDD). *Nat. Genet.*, **43**, 1189–1192.
9. Boyden, S.E., Mahoney, L.J., Kawahara, G., Myers, J.A., Mitsuhashi, S., Estrella, E.A., Duncan, A.R., Dey, F., DeChene, E.T., Blasko-Goehringer, J.M. *et al*. (2012) Mutations in the satellite cell gene MEGF10 cause a recessive congenital myopathy with minicores. *Neurogenetics*, **13**, 115–124.
10. Pierson, T.M., Markello, T., Accardi, J., Wolfe, L., Adams, D., Sincan, M., Tarazi, N.M., Fajardo, K.F., Cherukuri, P.F., Bajraktari, I. *et al*. (2013) Novel SNP array analysis and exome sequencing detect a homozygous exon 7 deletion of MEGF10 causing early onset myopathy, areflexia, respiratory distress and dysphagia (EMARDD). *Neuromuscul. Disord.*, **23**, 483–488.
11. Liewluck, T., Milone, M., Tian, X., Engel, A.G., Staff, N.P. and Wong, L.J. (2016) Adult-onset respiratory insufficiency, scoliosis, and distal joint hyperlaxity in patients with multiminicore disease due to novel Megf10 mutations. *Muscle Nerve*, **53**, 984–988.
12. Hartley, L., Kinali, M., Knight, R., Mercuri, E., Hubner, C., Bertini, E., Manzur, A.Y., Jimenez-Mallebrera, C., Sewry, C.A. and Muntoni, F. (2007) A congenital myopathy with diaphragmatic weakness not linked to the SMARD1 locus. *Neuromuscul. Disord.*, **17**, 174–179.
13. Mitsuhashi, S., Mitsuhashi, H., Alexander, M.S., Sugimoto, H. and Kang, P.B. (2013) Cysteine mutations cause defective tyrosine phosphorylation in MEGF10 myopathy. *F.E.B.S. Lett.*, **587**, 2952–2957.
14. Iram, T., Ramirez-Ortiz, Z., Byrne, M.H., Coleman, U.A., Kingery, N.D., Means, T.K., Frenkel, D. and El Khoury, J. (2016) Megf10 Is a Receptor for C1Q That Mediates Clearance of Apoptotic Cells by Astrocytes. *J. Neurosci.*, **36**, 5185–5192.
15. Draper, I., Mahoney, L.J., Mitsuhashi, S., Pacak, C.A., Salomon, R.N. and Kang, P.B. (2014) Silencing of drpr leads to muscle and brain degeneration in adult Drosophila. *Am. J. Pathol.*, **184**, 2653–2661.
16. Bröhl, D., Vasyutina, E., Czajkowski, Maciej, T., Griger, J., Rassek, C., Rahn, H.-P., Purfürst, B., Wende, H. and Birchmeier, C. (2012) Colonization of the satellite cell niche by skeletal muscle progenitor cells depends on Notch signals. *Dev. Cell*, **23**, 469–481.
17. Krivtsov, A.V., Rozov, F.N., Zinovyeva, M.V., Hendrikx, P.J., Jiang, Y., Visser, J.W. and Belyavsky, A.V. (2007) Jedi–a novel transmembrane protein expressed in early hematopoietic cells. *J. Cell Biochem.*, **101**, 767–784.
18. Luo, D., Renault, V.M. and Rando, T.A. (2005) The regulation of Notch signaling in muscle stem cell activation and postnatal myogenesis. *Semin. Cell Dev. Biol*, **16**, 612–622.
19. Sicinski, P., Geng, Y., Ryder-Cook, A.S., Barnard, E.A., Darlison, M.G. and Barnard, P.J. (1989) The molecular basis of muscular dystrophy in the mdx mouse: a point mutation. *Science*, **244**, 1578–1580.
20. Durbeej, M. and Campbell, K.P. (2002) Muscular dystrophies involving the dystrophin-glycoprotein complex: an overview of current mouse models. *Curr. Opin. Genet. Dev.*, **12**, 349–361.
21. Lu, A., Poddar, M., Tang, Y., Proto, J.D., Sohn, J., Mu, X., Oyster, N., Wang, B. and Huard, J. (2014) Rapid depletion of muscle progenitor cells in dystrophic mdx/utrophin(−/−) mice. *Hum. Mol. Genet.*, **23**, 4786–4800.
22. Kitzmann, M., Bonnieu, A., Duret, C., Vernus, B., Barro, M., Laoudj-Chenivesse, D., Verdi, J.M. and Carnac, G. (2006) Inhibition of Notch signaling induces myotube hypertrophy by recruiting a subpopulation of reserve cells. *J. Cell Physiol.*, **208**, 538–548.
23. Bulaj, G. (2005) Formation of disulfide bonds in proteins and peptides. *Biotechnol. Adv.*, **23**, 87–92.
24. Mossuto, M.F. (2013) Disulfide Bonding in Neurodegenerative Misfolding Diseases. *Int. J. Cell Biol.*, **2013**, 7.
25. Beltran-Valero de Bernabe, D., Voit, T., Longman, C., Steinbrecher, A., Straub, V., Yuva, Y., Herrmann, R., Sperner, J., Korenke, C., Diesen, C. *et al*. (2004) Mutations in the FKRP gene can cause muscle-eye-brain disease and Walker-Warburg syndrome. *J. Med. Genet.*, **41**, e61.
26. Gu, W.J., Corti, O., Araujo, F., Hampe, C., Jacquier, S., Lucking, C.B., Abbas, N., Duyckaerts, C., Rooney, T., Pradier, L. *et al*. (2003) The C289G and C418R missense mutations cause rapid sequestration of human Parkin into insoluble aggregates. *Neurobiol. Dis.*, **14**, 357–364.
27. Mourikis, P. and Tajbakhsh, S. (2014) Distinct contextual roles for Notch signalling in skeletal muscle stem cells. *B. M.C. Dev. Biol.*, **14**, 2.
28. Wen, Y., Bi, P., Liu, W., Asakura, A., Keller, C. and Kuang, S. (2012) Constitutive Notch activation upregulates Pax7 and promotes the self-renewal of skeletal muscle satellite cells. *Mol. Cell. Biol.*, **32**, 2300–2311.
29. Buas, M.F. and Kadesch, T. (2010) Regulation of skeletal myogenesis by Notch. *Exp. Cell Res.*, **316**, 3028–3033.
30. Bao, S. (2014) Notch controls cell adhesion in the drosophila eye. *PLoS. Genet.*, **10**, e1004087.
31. Gagan, J., Dey, B.K., Layer, R., Yan, Z. and Dutta, A. (2012) Notch3 and Mef2c proteins are mutually antagonistic via Mkp1 Protein and miR-1/206 MicroRNAs in differentiating myoblasts. *J. Biol. Chem.*, **287**, 40360–40370.
32. Wang, X.W., Xi, X.Q., Wu, J., Wan, Y.Y., Hui, H.X. and Cao, X.F. (2015) MicroRNA-206 attenuates tumor proliferation and

migration involving the downregulation of NOTCH3 in colorectal cancer. *Oncol. Rep.*, **33**, 1402–1410.
33. Shawber, C., Nofziger, D., Hsieh, J.J., Lindsell, C., Bogler, O., Hayward, D. and Weinmaster, G. (1996) Notch signaling inhibits muscle cell differentiation through a CBF1-independent pathway. *Development*, **122**, 3765–3773.
34. Evans, I.R., Rodrigues, F.S., Armitage, E.L. and Wood, W. (2015) Draper/CED-1 mediates an ancient damage response to control inflammatory blood cell migration in vivo. *Curr. Biol.*, **25**, 1606–1612.
35. Riesenberg, A.N. and Brown, N.L. (2016) Cell autonomous and nonautonomous requirements for Delltalike1 during early mouse retinal neurogenesis. *Dev. Dyn.*, **245**, 631–640.
36. Waddell, J.N., Zhang, P., Wen, Y., Gupta, S.K., Yevtodiyenko, A., Schmidt, J.V., Bidwell, C.A., Kumar, A. and Kuang, S. (2010) Dlk1 is necessary for proper skeletal muscle development and regeneration. *PLoS. One*, **5**, e15055.
37. Bray, S.J., Takada, S., Harrison, E., Shen, S.C. and Ferguson-Smith, A.C. (2008) The atypical mammalian ligand Delta-like homologue 1 (Dlk1) can regulate Notch signalling in Drosophila. *B.M.C. Dev. Biol.*, **8**, 11.
38. Eiraku, M., Tohgo, A., Ono, K., Kaneko, M., Fujishima, K., Hirano, T. and Kengaku, M. (2005) DNER acts as a neuron-specific Notch ligand during Bergmann glial development. *Nat. Neurosci.*, **8**, 873–880.
39. Nickoloff, B.J., Qin, J.Z., Chaturvedi, V., Denning, M.F., Bonish, B. and Miele, L. (2002) Jagged-1 mediated activation of notch signaling induces complete maturation of human keratinocytes through NF-kappa B and PPAR gamma. *Cell Death Differ.*, **9**, 842–855.
40. Wen, F., Wong, H.K., Tay, C.Y., Yu, H., Li, H., Yu, T., Tijore, A., Boey, F.Y.C., Venkatraman, S.S. and Tan, L.P. (2014) Induction of myogenic differentiation of human mesenchymal stem cells cultured on Notch Agonist (Jagged-1) modified biodegradable scaffold surface. *A.C. S. Appl. Mater. Interfaces*, **6**, 1652–1661.
41. Jung, J., Mo, J.-S., Kim, M.-Y., Ann, E.-J., Yoon, J.-H. and Park, H.-S. (2011) Regulation of Notch1 signaling by Delta-like ligand 1 intracellular domain through physical interaction. *Mol. Cells*, **32**, 161–165.
42. Sun, X. and Artavanis-Tsakonas, S. (1996) The intracellular deletions of Delta and Serrate define dominant negative forms of the Drosophila Notch ligands. *Development*, **122**, 2465–2474.
43. Dayanidhi, S. and Lieber, R.L. (2014) Skeletal muscle satellite cells: mediators of muscle growth during development and implications for developmental disorders. *Muscle Nerve*, **50**, 723–732.
44. Dumont, N.A., Wang, Y.X., von Maltzahn, J., Pasut, A., Bentzinger, C.F., Brun, C.E. and Rudnicki, M.A. (2015) Dystrophin expression in muscle stem cells regulates their polarity and asymmetric division. *Nat. Med.*, **21**, 1455–1463.
45. Vieira, N.M., Elvers, I., Alexander, M.S., Moreira, Y.B., Eran, A., Gomes, J.P., Marshall, J.L., Karlsson, E.K., Verjovski-Almeida, S., Lindblad-Toh, K. *et al.* (2015) Jagged 1 Rescues the Duchenne muscular dystrophy phenotype. *Cell*, **163**, 1204–1213.
46. Burdi, R., Rolland, J.-F., Fraysse, B., Litvinova, K., Cozzoli, A., Giannuzzi, V., Liantonio, A., Camerino, G.M., Sblendorio, V., Capogrosso, R.F. *et al.* (2009) Multiple pathological events in exercised dystrophic mdx mice are targeted by pentoxifylline: outcome of a large array of in vivo and ex vivo tests. *J. Appl. Physiol.*, **106**, 1311–1324.
47. Tinsley, J.M., Fairclough, R.J., Storer, R., Wilkes, F.J., Potter, A.C., Squire, S.E., Powell, D.S., Cozzoli, A., Capogrosso, R.F., Lambert, A. *et al.* (2011) Daily treatment with SMTC1100, a novel small molecule utrophin upregulator, dramatically reduces the dystrophic symptoms in the *mdx* Mouse. *PLoS One*, **6**, e19189.
48. Connolly, A.M., Keeling, R.M., Mehta, S., Pestronk, A. and Sanes, J.R. (2001) Three mouse models of muscular dystrophy: the natural history of strength and fatigue in dystrophin-, dystrophin/utrophin-, and laminin α2-deficient mice. *Neuromuscul. Disord.*, **11**, 703–712.
49. Lawson, M.A. and Purslow, P.P. (2000) Differentiation of myoblasts in serum-free media: effects of modified media are cell line-specific. *Cells Tissues Organs*, **167**, 130–137.
50. Der Vartanian, A., Audfray, A., Al Jaam, B., Janot, M., Legardinier, S., Maftah, A. and Germot, A. (2015) Protein O-fucosyltransferase 1 expression impacts myogenic C2C12 cell commitment via the Notch signaling pathway. *Mol. Cell Biol.*, **35**, 391–405.
51. Livak, K.J. and Schmittgen, T.D. (2001) Analysis of relative gene expression data using real-time quantitative PCR and the $2-\Delta\Delta CT$ method. *Methods*, **25**, 402–408.
52. Springer, M.L., Rando, T.A. and Blau, H.M. (2002) Gene delivery to muscle. *Curr. Protoc. Hum. Genet.*. doi: 10.1002/0471142905.hg1304s31.
53. Hulkower, K.I. and Herber, R.L. (2011) Cell migration and invasion assays as tools for drug discovery. *Pharmaceutics*, **3**, 107–124.
54. Bulfield, G., Siller, W.G., Wight, P.A. and Moore, K.J. (1984) X chromosome-linked muscular dystrophy (mdx) in the mouse. *Proc. Natl. Acad. Sci. U.S.A*, **81**, 1189–1192.
55. Alexander, M.S., Casar, J.C., Motohashi, N., Vieira, N.M., Eisenberg, I., Marshall, J.L., Gasperini, M.J., Lek, A., Myers, J.A., Estrella, E.A. *et al.* (2014) MicroRNA-486–dependent modulation of DOCK3/PTEN/AKT signaling pathways improves muscular dystrophy–associated symptoms. *J. Clin. Invest.*, **124**, 2651–2667.
56. Dunn, K.W., Kamocka, M.M. and McDonald, J.H. (2011) A practical guide to evaluating colocalization in biological microscopy. *Am. J. Physiol. Cell Physiol.*, **300**, C723–C742.
57. Bose, S.K., Sengupta, T.K., Bandyopadhyay, S. and Spicer, E.K. (2006) Identification of Ebp1 as a component of cytoplasmic bcl-2 mRNP (messenger ribonucleoprotein particle) complexes. *Biochem. J.*, **396**, 99–107.
58. Poole, A.R. and Hebert, M.D. (2016) SMN and coilin negatively regulate dyskerin association with telomerase RNA. *Biol. Open*, **5**, 726–735.